JOC The Journal of Organic Chemistry

Article

pubs.acs.org/joc

DFT Study on the Mechanisms and Stereoselectivities of the [4 + 2] Cycloadditions of Enals and Chalcones Catalyzed by N-Heterocyclic Carbene

Zhenyu Li, Donghui Wei,* Yang Wang, Yanyan Zhu,* and Mingsheng Tang

The College of Chemistry and Molecular Engineering, Center of Computational Chemistry, Zhengzhou University, Zhengzhou, Henan Province, 450001, P.R. China

Supporting Information

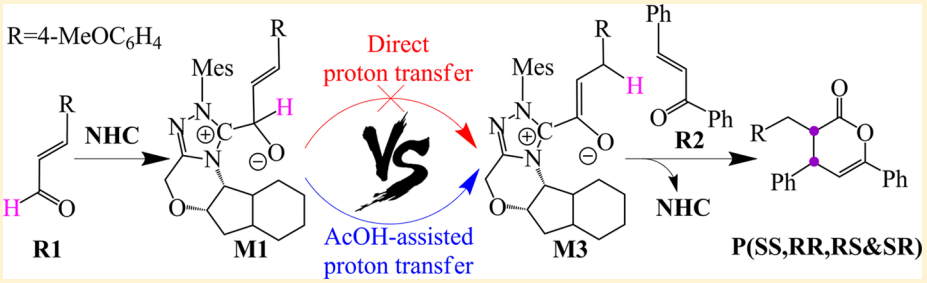

ABSTRACT: The possible reaction mechanisms of stereoselective [4 + 2] cycloaddition of enals and chalcones catalyzed by N-heterocyclic carbene (NHC) have been investigated using density functional theory (DFT). The calculated results indicate that the most favorable reaction channel occurs through five steps. The first step is the nucleophilic attack on the enal by NHC. Then, there are two consecutive acid (AcOH)-assisted proton-transfer steps. Subsequently, the fourth step is the [4 + 2] cycloaddition process associated with the formation of two chiral centers, followed by dissociation of NHC and product. Our computational results demonstrate that the [4 + 2] cycloaddition is the rate-determining and stereoselectivity-determining step. The energy barrier for the SS configurational channel (17.62 kcal/mol) is the lowest one, indicating the SS configurational product should be the main product, which is in agreement with experiment. Moreover, the role of NHC catalyst in the [4 + 2] cycloaddition of enal and chalcone was explored by the analysis of global reactivity indexes. This work should be helpful for realizing the significant roles of catalyst NHC and the additive AcOH and thus provide valuable insights on the rational design of potential catalyst for this kind of reactions.

1. INTRODUCTION

Since Arduengo and co-workers opened access to free, isolable N-heterocyclic carbenes (NHCs) in 1991,[1] NHCs have attracted more and more attention becuase of their high and special activity. The NHCs can coordinate not only to transition metals but also to beryllium, sulfur, iodine, and many other main group elements.[2−5] Because of their specific coordination activity, the NHCs can both stabilize and activate metal centers in quite different key catalytic steps of organic syntheses, for example, C−H activation, C−C bond formation, etc.[2] Recently, chemists also discovered that NHCs could exhibit promising properties as one unique class of organocatalysts for a number of reactions in organic chemistry.[6−10] To avoid the cost of the transition-metal catalysis and the toxicity of the heavy metals, the field of organocatalysis has been rapidly developing in recent years, and organocatalysts are excellent from the viewpoint of reaction diversity, high enantioselectivity, and design flexibility.[11−16] As an important kind of Lewis base organocatalysts, NHCs have attracted a vast amount of interest from organic chemists[17,18] To date, various C−C bond formations have been achieved by NHC organocatalysts,[6,19] such as the benzoin reaction,[20−23] the Stetter reaction,[24−26] homoenolate reactions,[27−29] and cycloaddition reactions.[30−32]

It is noteworthy that NHCs have been found to be efficient organocatalysts for enantioselective cycloaddition reactions in the past several years.[30,33−39] In particular, Ye et al. reported a series of highly enantioselective cycloaddition reactions catalyzed by NHCs, including the [2 + 2] cycloaddition of ketenes and imines,[33] the [2 + 2] cycloaddition of ketenes and dicarboxylates,[34] the [4 + 2] cycloaddition of ketenes and oxindoles,[30] the [2 + 2 + 2] cycloaddition reaction of ketenes and carbon disulfides,[35] and the [3 + 2] annulation of enals and isatins.[36] In addition, Chi and co-workers have studied the NHC-catalyzed enal cycloaddition reactions, such as the Diels−Alder reactions of enals and diketones,[37] the reactions of enals and unsaturated imines to generate spirocyclicoxindoles,[38] and the oxidative additions of enals and ketones.[39]

Because of the special reactivities and broad applications of the NHC-catalyzed reactions (especially the cycloaddition reactions), they have also drawn increasing attention from

Received: January 26, 2014
Published: March 16, 2014

   dx.doi.org/10.1021/jo500194d | J. Org. Chem. 2014, 79, 3069−3078

theoretical chemists.[40−43] For example, Kuniyil and Sunoj used DFT (M06-2X) method to study the NHC-catalyzed Stetter reaction and the enantioselectivities.[43] Notably, the reaction mechanisms and the role of NHC catalyst may be diverse in different NHC-catalyzed cycloadditions,[41] which is due to the different reactants and their special activities. For example, we have studied the mechanisms for enantioselective synthesis via NHC-catalyzed ketene [2 + 2],[40] [4 + 2],[41] and [2 + 2 + 2][42] cycloaddition reactions using the DFT methods, and we found that these cycloaddition reactions do not always originate from the reaction of NHC catalysts and the ketene. Therefore, people cannot conclude the real role of catalyst NHCs in those cycloadditions by experience.

In 2013, Chi et al. reported that the [4 + 2] cycloadditions of enals and chalcones catalyzed by NHCs can lead to enolate-type lactone products in good yields with excellent ee (enantiomeric excess) values (Scheme 1).[44] However, the theoretical investigation on the mechanisms of this type of reactions is not available in the literature, and the detailed reaction mechanisms and the real roles of catalyst NHCs remain unclear. It should be noted that this reaction includes the proton-transfer processes and therefore is obviously different from the NHC-catalyzed ketene cycloaddition reactions discussed above. Moreover, the reaction occurs in the presence of the additive (AcOH), as the protic additive/media-assisted proton transfer can occur more easily than the direct proton transfer.[45−47] Thus, we proposed that besides the direct proton-transfer pathway, an AcOH-assisted proton transfer pathway may also exist. In addition, the different NHC-catalyzed cycloaddition reaction system might lead to the diversity of the manner, position, and even order for the complexation of NHC and reactants.[40,41] Consequently, we should also consider the different possible pathways to explore why the title reaction cannot take place without the catalyst NHC. This prompted us to do a theoretical study on the possible mechanisms and the stereoselectivities of the organo-catalytic reaction and make clear how and why the reaction can occur under the mild conditions (room temperature) in the presence of NHCs. It is noteworthy that this work is remarkably different from the previous theoretical studies on the NHC-catalyzed ketene cycloadditions since there is not any proton transfer process involved in those studies. We believe this work would be helpful for people to understand the detailed mechanisms and the real roles of the additive and NHC catalyst in this type of reactions.

Scheme 1. NHC-Catalyzed [4 + 2] Cycloaddition of Enals and Chalcones

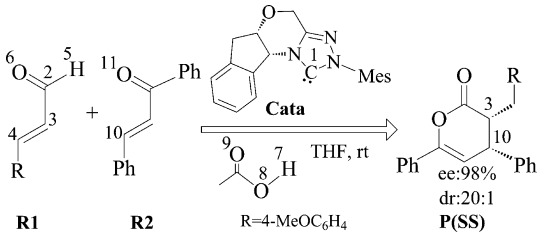

The [4 + 2] cycloaddition of the enal **R1** and chalcone **R2** catalyzed by NHC **Cata** to form the SS configurational product **P(SS)** with 98% ee (Scheme 1)[44] has been chosen as the object of this study. As shown in Scheme 1, it should be noted that there are two chiral centers (C3 and C10) in the main product **P(SS)**; we use the first letter in parentheses to represent the chirality of C3 atom and the second letter to represent the chirality of C10 atom. The following suffixes of the stationary points have the same meaning. The reaction mechanisms were studied using density functional theory (DFT), which has been widely applied to studies of reaction mechanisms.[43,48−57]

2. COMPUTATIONAL DETAILS

All theoretical calculations were performed using the Gaussian 09 program.[58] The previous studies[40,41,59−62] indicated that the B3LYP[63,64] functional calculations account well for the experimental results. All structures of the reactants, intermediates, transition states, and products were optimized at the B3LYP/6-31G(d, p) level of theory in the THF solvent simulated by the integral equation formalism polarizable continuum model (IEF-PCM).[65,66] Based on the experiment reported by Chi and co-workers, KOAc and AcOH are the additives and THF is the solvent of the reaction, so we did not consider the solvent effect of them. The results of frequency

Scheme 2. Possible Catalytic Cycle of the Title Reaction

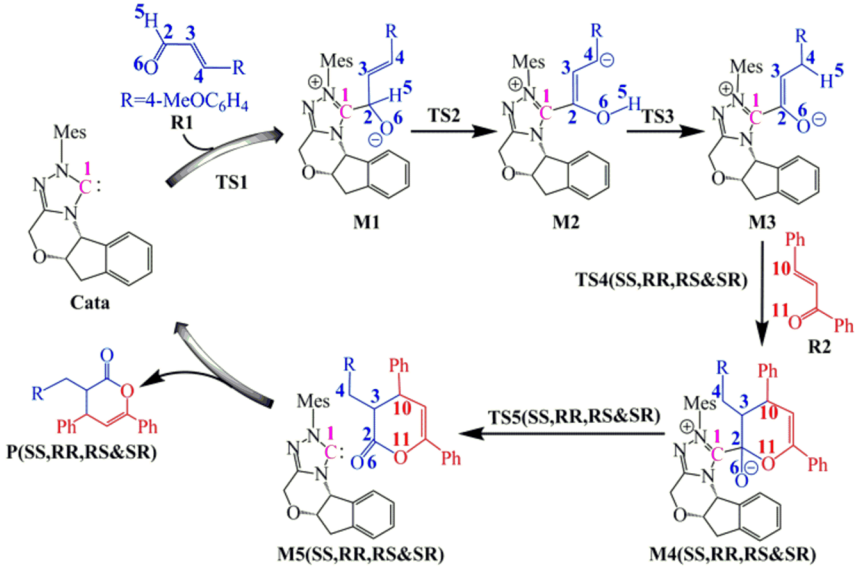

dx.doi.org/10.1021/jo500194d | J. Org. Chem. 2014, 79, 3069−3078

Scheme 3. Possible Reaction Mechanisms for the Second and Third Steps Catalyzed by Cata

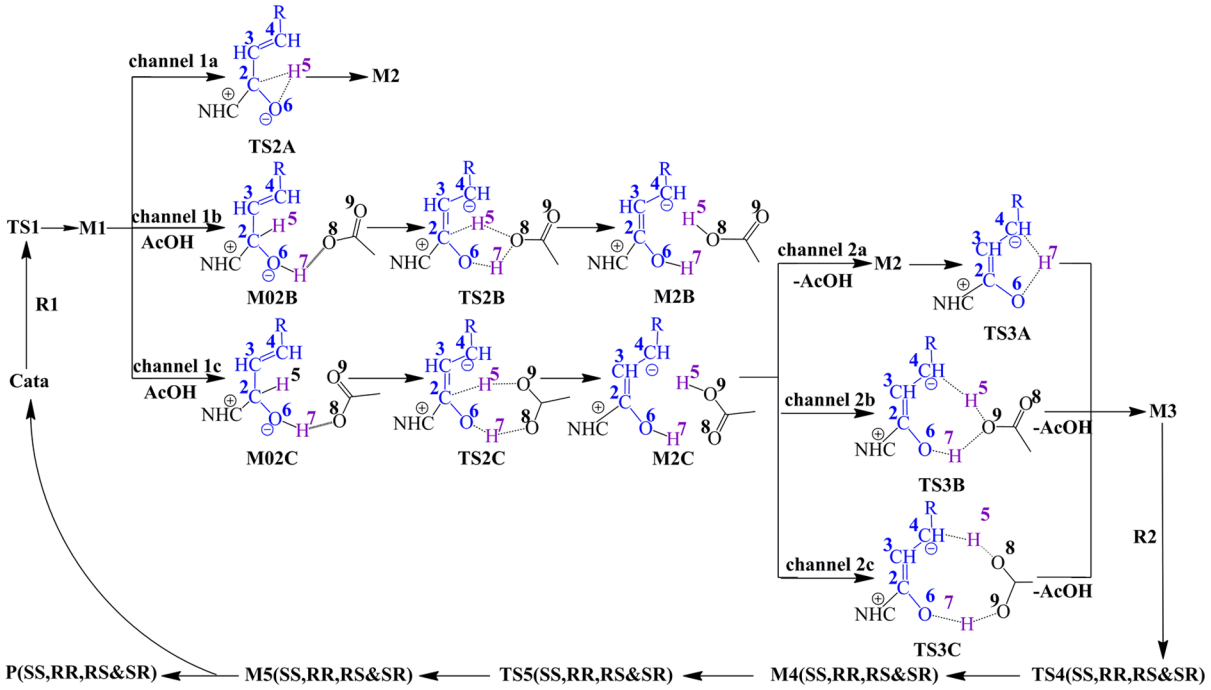

calculations show that all minima structures have no imaginary frequency and each transition state has only one imaginary frequency. All the energies discussed in this paper include the zero-point vibrational energy (ZPVE) corrections obtained from the frequency calculation at the B3LYP/6-31G(d, p) level in the solvent.

3. RESULTS AND DISCUSSION

In this work, we have suggested and investigated two possible pathways for the [4 + 2] cycloaddition reaction of enals and chalcones, which have been discussed in detail as follows:

3.1. The First Reaction Pathway. As can be seen in Scheme 2, there are five steps in the reaction cycle catalyzed by **Cata**, including (1) the combination of **R1** and **Cata**; (2) the proton transfers from C2 to O6; (3) the proton transfers from O6 to C4; (4) the [4 + 2] cycloaddition of **M3** with **R2** to form two chiral centers (i.e., C3 and C10 atoms) and four kinds of stereoisomers; and (5) the dissociation of **Cata** and products. Notably, there is more than one possible channel for the second and third steps, and a brief summary and illustration is shown in Scheme 3.

3.1.1. First Step: Complexation of NHC to R1. As shown in Scheme 2, the nucleophilic attack on the C2 atom of **R1** by C1 atom of **Cata** forms intermediate **M1** via transition state **TS1**. Figure 1 shows all the optimized structures involved in steps 1−3. The distance between the C1 and C2 atoms is shortened from 1.947 Å in **TS1** to 1.545 Å in **M1**, indicating the fully formation of the C1−C2 bond in NHC-enal adduct **M1**.

3.1.2. Second Step: Proton Transfer from C2 to O6. As depicted in Scheme 3, there are three possible channels for the second reaction step: the proton H5 transfers from C2 to O6 directly via the three-membered transition state **TS2A** (channel 1a), the proton H5 transfers from C2 to O6 with the help of acetic acid (AcOH) via a five-membered ring transition state **TS2B** (channel 1b), or there is a seven-membered ring transition state **TS2C** (channel 1c).

As shown in Figure 1, the distance change of C2−H5 indicates the breaking of the C2−H5 bond, whereas the distance change of O6−H5 shows that a new bond is formed in channel 1a. Moreover, the bond length of C2−O6 is 1.339, 1.453, and 1.405 Å in **M1**, **TS2A**, and **M2**, respectively. Notably, the dihedral angle of C1−O6−C2−C3 is 179.67° in **M2**, which shows that the four atoms are coplanar. The coordination number of C2 changes from four in **TS2A** to three in **M2**, and the hybridization of C2 changes from sp^3 in **TS2A** to sp^2 in **M2**. The difference in the bond length of C2−O6 can be attributed to the greater s-character in the C2−O6 bond in **M2** over that in **M1**.

For channel 1b, we denote the precursor as **M02B** (depicted in Scheme 3), and there is an intermediate **M2B** to be generated in this step. As can be seen from Figure 1, the distance changes of C2−H5 and O8−H7 indicate the breaking of the two bonds, while the distance changes of O8−H5 and O6−H7 show the formation of the bonds O8−H5, O6−H7 in the structural transformation process from **M02B** to **M2B** via **TS2B**.

In channel 1c, we denote the precursor as **M02C** (depicted in Scheme 3). As shown in Figure 1, the distances of C2−H5 and O8−H7 are lengthened from 1.101 and 1.478 Å in **M02C** to 2.071 and 1.841 Å in **M2C**, respectively, while the distance changes of O6−H7 and O9−H5 illustrate the formation of the two bonds in the structural transformation process from **M02C** to **M2C** via **TS2C**.

We set the energies of **R1+R2+Cata+AcOH** as 0.00 kcal/mol as references in the three channels (Figure 2). The energy barriers of channels 1a (black line), 1b (red line), and 1c (blue line) are 36.11, 16.73, and 10.63 kcal/mol, respectively. Channel 1c has the lowest energy barrier among the three channels and, therefore, is more energetically favorable than the others.

As shown in Figure 1, hydrogen bond O6−H7···O8 exists in both **M02B** (channel 1b) and **M02C** (channel 1c); this explains why their energies are dramatically lower than that of **M1**. A weak hydrogen bond O6−H7···O8 exists in transition state **TS2B**, where the distances of O6−H7 and O8−H7 are

dx.doi.org/10.1021/jo500194d | J. Org. Chem. 2014, 79, 3069−3078

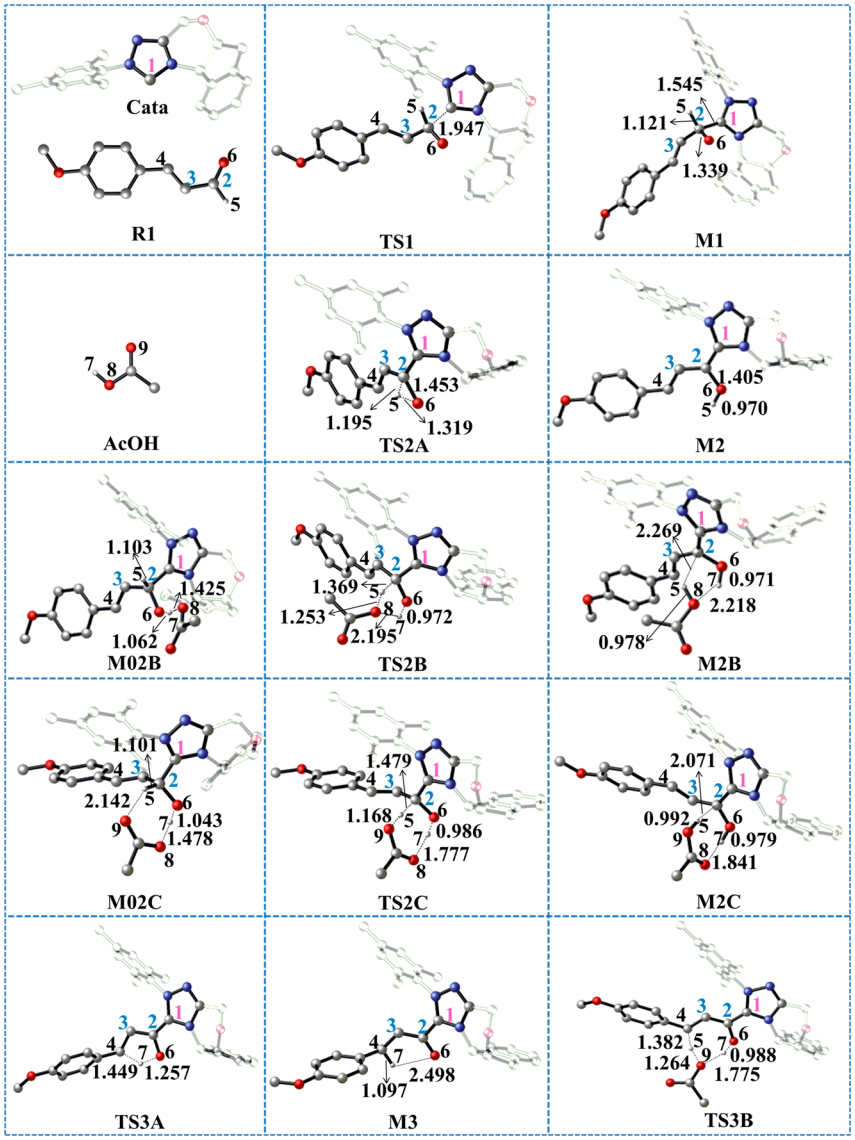

Figure 1. Optimized geometries of all stationary points involved in steps 1−3 (the hydrogen atoms which are not involved in the reaction are omitted; the substituted groups of **Cata** are shown in transparent; distances in angstroms).

0.972 and 2.195 Å and the angle of O6−H7−O8 is 121.71°. Similarly, in transition state **TS2C**, the distances of O6−H7 and O8−H7 are 0.986 and 1.777 Å and the angle of O6−H7−O8 is 161.85°. We believe the main reason that **TS2C** has a lower energy than **TS2B** is attributed to the stronger hydrogen bond O6−H7···O8 in **TS2C** than that in **TS2B**.

3.1.3. Third Step: Proton Transfer from O6 to C4. As shown in Scheme 3, there are three possible channels in the third step: the proton H7 transfers from O6 to C4 directly (channel 2a) or H7 transfers with the help of acetic acid (AcOH) (including channels 2b and 2c).

Channel 2a is a process where H7 transfers directly via a five-membered ring (C4−H7−O6−C2−C3) transition state **TS3A** (depicted in Figure 1). The distance of O6−H7 is lengthened from 1.257 Å in **TS3A** to 2.498 Å in **M3**, while the distance of C4−H7 is shortened from 1.449 Å in **TS3A** to 1.097 Å in **M3**, indicating the breaking of O6−H7 bond and the formation of C4−H7 bond.

For channel 2b, the proton H7 transfers from O6 to O9 and H5 transfers from O9 to C4 via a seven-membered ring (C4−H5−O9−H7−O6−C2−C3) transition state **TS3B**. As we can see from Figure 1, the distances of O6−H7, O9−H7, C4−H5, and O9−H5 are 0.988, 1.775, 1.382, and 1.264 Å in **TS3B**, respectively. Although we have tried many times, perhaps due to the strain of nine-membered ring, the expected transition state **TS3C** could not be located, therefore, we did not discuss this channel in this study.

In Figure 3, we still set the energies of **R1**+**R2**+**Cata**+**AcOH** as 0.00 kcal/mol as references. The energy barrier of channel 2a (black line) is 23.96 kcal/mol, but the energy barrier of channel 2b (red line) is 5.21 kcal/mol. Channel 2b has a much lower energy barrier than that of channel 2a, and therefore is more energetically favorable.

3.1.4. Fourth Step: Ring-Closure Reaction ([4 + 2] Cycloaddition). As shown in Scheme 2, this step is to form the six-membered (oxygen)-heterocycle structure that can be found in the final product, so **M3** needs to react with **R2** via [4 + 2] cycloaddition. Scheme 4 illustrates stereochemistry of this step (the *Si* or *Re* face of **M3** is in terms of the prochiral atom C3, and the *Si* or *Re* face of **R2** is in terms of the prochiral atom

dx.doi.org/10.1021/jo500194d | J. Org. Chem. 2014, 79, 3069−3078

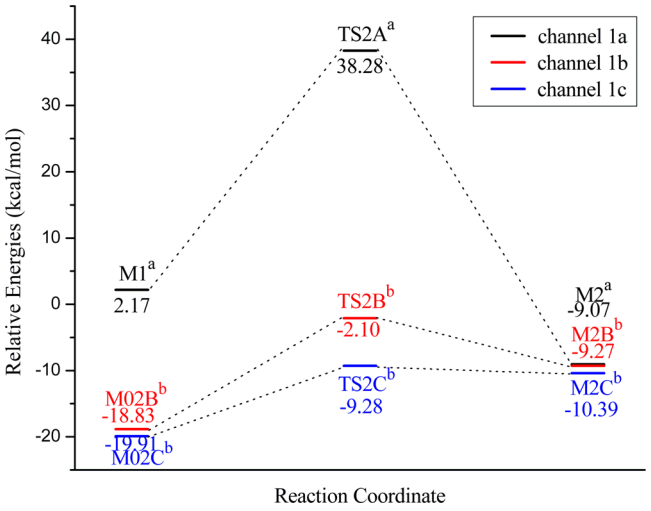

Figure 2. Energy profiles of the three channels in the second step (unit: kcal/mol, the superscript "a" represents adding the energies of **AcOH** and **R2**, the superscript "b" represents adding the energy of **R2**).

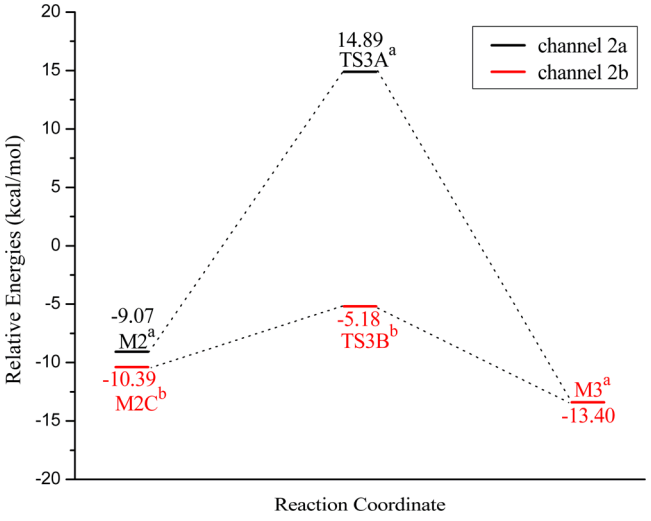

Figure 3. Energy profiles of the two possible channels in the third step (unit: kcal/mol, the superscript "a" represents adding the energies of **AcOH** and **R2**, the superscript "b" represents adding the energy of **R2**).

C10). During this step, four possible reaction patterns can take place (Table 1). The attack from the *Re* face of **M3** on the *Re* or *Si* face of **R2** leads to the formation of intermediates **M4(SS)** and **M4(SR)**, respectively, whereas the attack from the *Si* face of **M3** on the *Re* or *Si* face of **R2** leads to intermediates **M4(RS)** and **M4(RR)**, respectively. Therefore, there are four different kinds of stereoisomers, i.e., SS, SR, RS, and RR, in this [4 + 2] cycloaddition process.

With the approaching of **M3** to **R2**, the six-membered ring is formed in **M4(SS,RR,RS/SR)** via transition state **TS4(SS,RR,RS/SR)**. Figure 4 shows the structures and geometrical parameters of the transition states and intermediates involved in the fourth and fifth steps. As depicted in Figure 4, the distance changes of C2−O11 and C3−C10 confirm the formation of the six-membered ring in all the four configurations.

3.1.5. Fifth Step: the Dissociation of Catalyst and Products. In this step, catalyst **Cata** is dissociated with the

Scheme 4. Stereochemistry of the [4 + 2] Cycloaddition in the Fourth Step

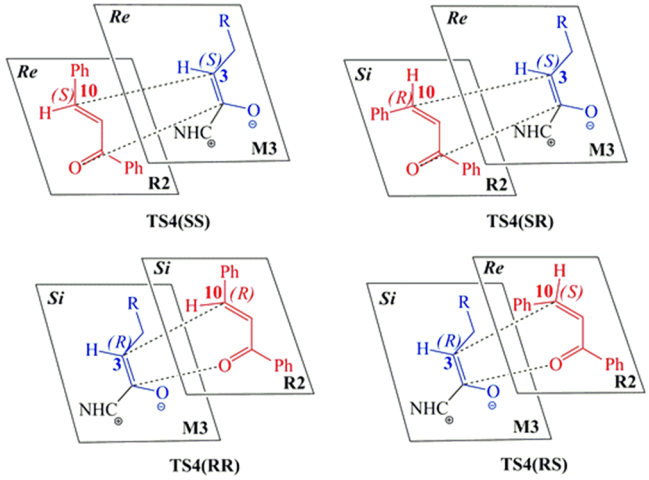

Table 1. Four Possible Reaction Patterns for the Fourth Step

addition face of **M3**	addition face of **R2**	configuration of **M4**
Re	*Re*	*SS*
Re	*Si*	*SR*
Si	*Re*	*RS*
Si	*Si*	*RR*

product via transition state **TS5(SS,RR,RS/SR)**. As depicted in Figure 4, the distance of C1−C2 is lengthened from 1.591/1.579/1.587/1.603 Å in **M4(SS,RR,RS/SR)** to 1.959/2.012/2.106/2.076 Å in **TS5(SS,RR,RS/SR)**. **M5(SS,RR,RS/SR)** consists of two segments, i.e., the catalyst **Cata** and the product **P(SS,RR,RS/SR)**. Moreover, the distance of C1−C2 is 3.431/3.856/3.772/3.859 Å in **M5(SS,RR,RS/SR)**, implying that it can dissociate easily to form the product and the catalyst **Cata**.

Taking all five steps of the [4 + 2] cycloaddition reaction catalyzed by **Cata** into consideration, the most favorable channels for the second and third step are channels 1c and 2b. In Figure 5, we have summarized the energy profiles of the most favorable reaction pathway and also set the energies of **R1+R2+Cata+AcOH** as 0.00 kcal/mol as references.

Figure 5 shows that the energy barriers of the first, second, and third steps are 8.22, 10.63, and 5.21 kcal/mol, respectively, which are low enough for the reaction to take place at room temperature. The fourth step, i.e., the [4 + 2] cycloaddition, is the rate-determining step, and it determines the stereoselectivities (SS-favorable) associated with the chiral carbon atoms C3 and C10. The energy barriers of the fourth step are 17.62 (**TS4(SS)**), 19.65 (**TS4(RR)**), 19.03 (**TS4(RS)**), and 19.77 (**TS4(SR)**) kcal/mol, respectively, which implies all of the four isomers can be formed at room temperature. The energy barrier via **TS4(SS)** (17.62 kcal/mol) is the lowest one among the four channels; hence, **M4(SS)** is the most favorable isomer from the aspect of kinetics. Moreover, the difference of energy barrier between the SS and RR configuration in this step is 2.03 kcal/mol. This value corresponds to an enantiomeric excess of about 94%,[67,68] which is very close to the experimental outcome (98% ee).[44] This agreement demonstrates that the computational method utilized in the present work, including the density functional, basis set, and solvation model, is suitable for the title reaction system. Finally, the

dx.doi.org/10.1021/jo500194d | J. Org. Chem. 2014, 79, 3069−3078

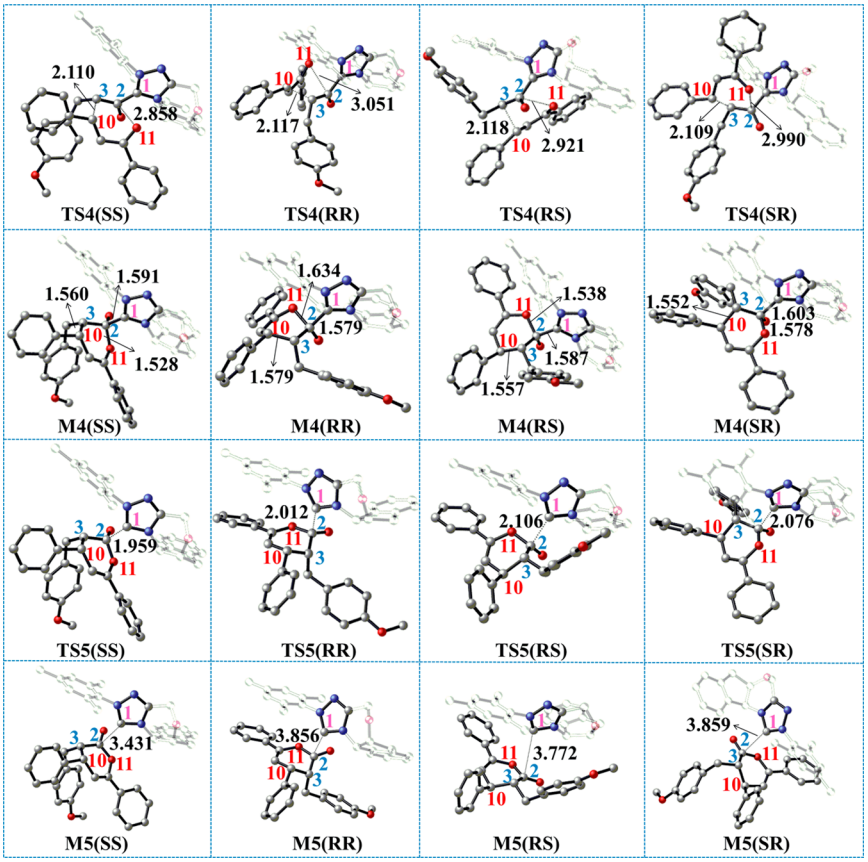

Figure 4. Optimized geometries of the stationary points in the fourth and fifth steps (the hydrogen atoms which are not involved in the reaction are omitted; the substituted groups of Cata are shown in transparent; distances in angstroms).

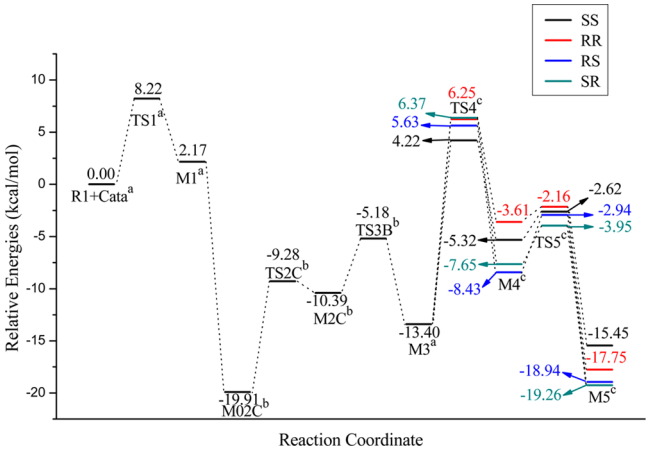

Figure 5. Energy profiles of the entire NHC-catalyzed reaction (unit: kcal/mol, the superscript "a" represents adding the energies of **AcOH** and **R2**, the superscript "b" represents adding the energy of **R2**, and the superscript "c" represents adding the energy of **AcOH**).

energy barriers of the fifth step are only 2.70 (**TS5(SS)**), 1.45 (**TS5(RR)**), 5.49 (**TS5(RS)**), and 3.70 (**TS5(SR)**) kcal/mol, respectively, which indicates that the catalyst is easy to regenerate.

The energy of **M5(SS,RR,RS/SR)** is 15.45/17.75/18.94/19.26 kcal/mol lower than those of the reactants, therefore, the overall reaction is an exothermic process. Though the intermediate **M02C** is the lowest point on the energy profiles, the energy barrier of the entire reaction is not high that the intermediate **M02C** can easily transform to the intermediate **M5(SS,RR,RS/SR)**, which would be dissociated to catalyst and products quickly in experiment.

3.1.6. The Possible Channels Associated with the Structural Transformation from M1 to M3. Besides the reaction mechanisms proposed and discussed above, we have also studied an alternative possible proton-transfer mechanism to produce **M3** from **M1** directly. Scheme 5 exhibits three possible channels (channels 3a, 3b, and 3c) that will be

Scheme 5. Possible Proton-Transfer Channels Associated with the Structural Transformation from M1 to M3

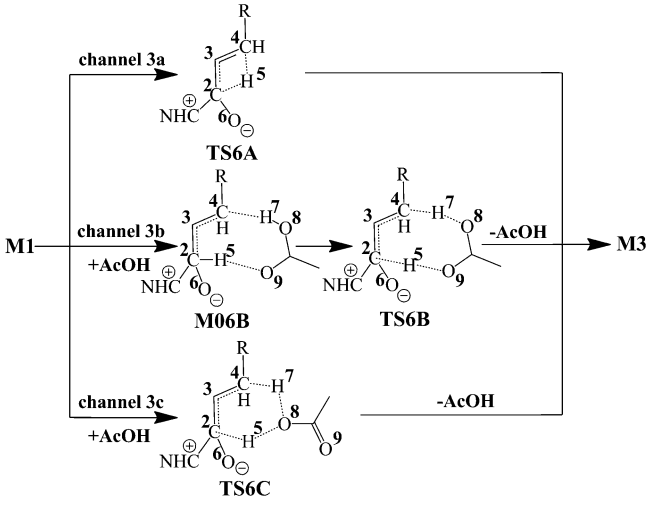

dx.doi.org/10.1021/jo500194d | J. Org. Chem. 2014, 79, 3069−3078

discussed in this section. We have tried for many times, but the transition state **TS6C** proposed in channel 3c was not located. We denote the precursor of channel 3b as **M06B** and set the energy of **M1**+**AcOH** as 0.00 kcal/mol as references. The calculated energy barriers of channels 3a and 3b are 73.20 and 25.81 kcal/mol, respectively, which are higher than those of the favorable channels 1c and 2b described above. Thus, the favorable channels should be channels 1c and 2b for the title reaction.

3.2. Second Possible Pathway. In this paper, we have suggested two different mechanisms (the first and second pathways) due to the two different reaction modes between NHC and the reactants, i.e., NHC reacts with enal in the first step (enal-first mechanism) and NHC reacts with chalcone in the first step (chalcone-first mechanism). In the second pathway, it should be noted that **Cata** reacts with **R2**, and **R1** should change into ketene via the proton-transfer process so as to complete the [4 + 2] cycloaddition reaction. Thus, we had to study the possibility of the structural transformation from **R1** to ketene intermediate.

For the structural transformation from **R1** to ketene intermediate, we proposed three possible channels (Scheme 6): the proton H5 transfers from C2 to C4 via 1,3-sigmatropic

Scheme 6. Possibility of R1 Transforming to Ketene in the Second Pathway

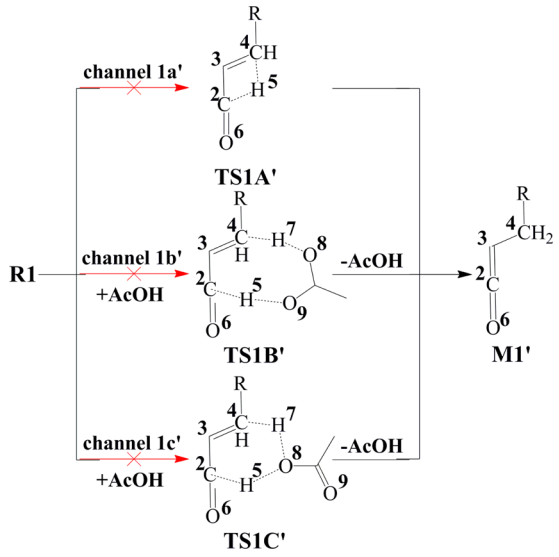

hydrogen shift directly via **TS1A′** (channel 1a′) or proton transfers from C2 to C4 with the help of AcOH via an eight-membered ring transition state **TS1B′** (channel 1b′) or a six-membered ring transition state **TS1C′** (channel 1c′). The transition states **TS1A′** and **TS1B′** have been obtained, but **TS1C′** proposed in channel 1c′ was not located. We set the energy of **R1**+**AcOH** as 0.00 kcal/mol as reference. The calculated energy barriers of channels 1a′ (62.43 kcal/mol) and 1b′ (54.01 kcal/mol) are too high for this reaction to occur via this pathway at room temperature. Therefore, we think it should be useless to consider the following reaction processes of this pathway.

In addition to the energy barriers, we have found that the structures of transition states should be responsible for the unfavorability of the second pathway. As for **TS1A′**, the strong strain of four-membered ring makes **TS1A′** very unstable. Moreover, we have performed the distortion/interaction analysis[69] to explain the high energy barrier via **TS1B′**. The distortion/interaction analysis developed by Houk and co-workers provides a highly insightful method for understanding reactivity and activation barriers in the cycloadditions. Here the activation energy is divided into two main components, the distortion (E_{dis}) and interaction (E_{int}) energies. The distortion energy involves geometric and electronic changes to deform the reactants into their transition state geometry, which contains bond stretching, angle decrease or increase, dihedral change, and so on. The interaction energy includes repulsive exchange-repulsive and stabilizing electrostatic, polarization, and orbital effects in the transition state structure. As shown in Figure 6,

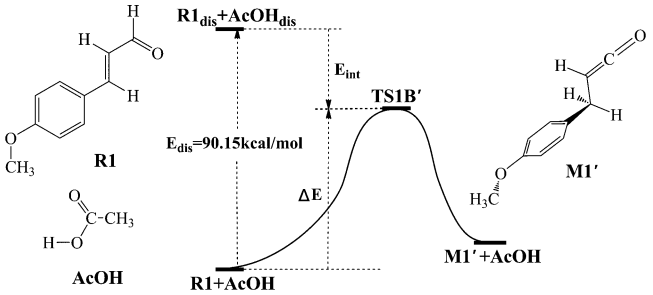

Figure 6. Distortion/interaction analysis for channel 1b′.

the distortion energy E_{dis} (90.15 kcal/mol) is too high for the interaction energy to neutralize, which leads to the extremely high energy barrier of channel 1b′. All these factors would make the structural transformation from **R1** to **M1′** difficult.

Compared with our previous theoretical studies on the NHC-catalyzed ketene cycloadditions,[40−42] it should be mentioned that NHC plays a special and very important role in the proton-transfer processes of this reaction. Based on the above results, we conclude that the NHC has to combine with **R1** instead of **R2** in order for the reaction to take place under the experimental conditions.

3.3. Analysis of the Global Reactivity Indexes of the Reactants. In order to better understand the role of Lewis base catalyst NHC, we have performed the analysis of global reactivity indexes of the reactants. As shown in Table 2, the

Table 2. Energy of HOMO (E_H, in au), Energy of LUMO (E_L, in au), Electronic Chemical Potential (μ, in au), Chemical Hardness (η, in au), Global Electrophilicity (ω, in eV), and Global Nucleophilicity (N, in eV) of Some Reactants (SR)

SR	E_H (au)	E_L (au)	μ (au)	η (au)	ω (eV)	N (eV)
R1	−0.218	−0.075	−0.146	0.144	2.029	2.875
R2	−0.234	−0.083	−0.1585	0.152	2.250	2.436
M1	−0.184	−0.027	−0.106	0.157	0.970	3.809

molecular global electrophilicity character is measured by electrophilicity index ω,[70] which is calculated by the following expression, $\omega = (\mu^2/2\eta)$,[70−74] in terms of the electronic chemical potential μ and the chemical hardness η. Both quantities may be approached in terms of the one-electron energies of the frontier molecular orbital HOMO and LUMO, E_H and E_L, as $\mu \approx (E_H + E_L)/2$ and $\eta \approx (E_L - E_H)$.

According to the HOMO energies obtained within the Kohn−Sham scheme,[75−77] Domingo and co-workers developed

dx.doi.org/10.1021/jo500194d | J. Org. Chem. 2014, 79, 3069−3078

the nucleophilicity index N to handle a nucleophilicity scale.[78−84] The nucleophilicity index is defined as $N = E_{HOMO(SR)} - E_{HOMO(TCE)}$. The nucleophilicity scale is referred to tetracyanothylene (TCE) taken as a reference. Following the definition of indices, in this reaction, **M1** is classified as the nucleophile (N = 3.809 eV), where **R2** is an electrophile with the ω value of 2.250 eV. The nucleophilicity of **M1** is obviously stronger than that of **R1**, indicating that Lewis base organocatalyst NHC noticeably strengthens the nucleophilicity of the reactant **R1** after the combination, and thus makes it easier for the cycloaddition reaction to take place.

4. CONCLUSION

In this paper, the reaction mechanisms of stereoselective [4 + 2] cycloaddition of enals and chalcones catalyzed by N-heterocyclic carbene (NHC) have been explored for the first time using the DFT method. We have suggested and studied two possible pathways of the NHC-catalyzed enal-chalcone [4 + 2] cycloaddition reaction to form four kinds of stereoisomers at the B3LYP/6-31G(d, p) level in THF solvent using IEF-PCM model. Several possible proton-transfer channels, including direct and AcOH-assisted proton-transfer channels, have been suggested and investigated. The computational results show that the additive AcOH plays an important role to make the proton transfer easier to take place. We found that the NHC also plays a significant role in the proton-transfer process, which is remarkably different from the NHC-catalyzed ketene cycloaddition reactions. The calculated results indicate that the most favorable pathway involves the following five reaction steps: catalyst NHC reacts with enal R1 to initiate the reaction, followed by two consecutive proton transfer processes via channels 1c and 2b to generate intermediate M3. Subsequently, the fourth step is the [4 + 2] cycloaddition via four different stereoselective channels (SS, RR, RS, and SR). Finally, the NHC Cata is dissociated with the product and the catalytic cycle is completed.

Notably, the fourth step is demonstrated to be the rate-determining step, as the stereoselectivities associated with the two chiral carbon centers (C3 and C10 atoms) are determined in this step as well. The computational results reveal that the product with SS configuration is the major stereoisomer, and the energy barrier associated with the SS configuration in this step is low enough to overcome at the room temperature. In addition, we have also compared the difference between the energy barriers of SS and RR configurations in the stereoselectivity-determining step (2.03 kcal/mol), which corresponds to an enantiomeric excess of about 94%, this is in good agreement with the experimental ee value (98%). Furthermore, the analysis of global reactivity indexes confirms that the organocatalyst NHC is a Lewis base and noticeably strengthens the nucleophilicity of the reactant **R1**, thus promoting the [4 + 2] cycloaddition reaction. The novel mechanistic insights obtained in the present study should be valuable for rational design of the more efficient NHC catalysts to achieve highly stereoselective enal [4 + 2] cycloadditions.

5. APPENDIX

The geometry optimization and frequency analysis of the key transition state **TS4(SS,RR,RS/SR)** were also performed at the M06-2X[85,86]/6-31G(d, p) level with solvent THF. The geometries of the transition states optimized by the two methods (B3LYP and M06-2X) have tiny differences. In order to compare the relative energies of the four transition states optimized by the two methods, we set the energy of **TS4(SS)** as 0.00 kcal/mol as references in Table 3. As can be seen in Table 3, the transition state **TS4(SS)** has the lowest energy at both the B3LYP/6-31G(d, p) and M06-2X/6-31G(d, p) levels, therefore, SS configurational product should be the major product, which indicates that our calculated results are in agreement with the experiment and should be reasonable.

Table 3. Relative Energies of TS4(SS, RR, RS/SR) Calculated at the B3LYP/6-31G(d, p) and M06-2X/6-31G(d, p) Levels (kcal/mol)

	B3LYP	M06-2X
TS4(SS)	0.00	0.00
TS4(RR)	2.03	2.68
TS4(RS)	1.41	3.98
TS4(SR)	2.15	2.59

■ ASSOCIATED CONTENT

Supporting Information

Cartesian coordinates as well as total energies and ZPVE for all the optimized structures. This material is available free of charge via the Internet at http://pubs.acs.org.

■ AUTHOR INFORMATION

Corresponding Authors

*E-mail: donghuiwei@zzu.edu.cn.
*E-mail: zhuyan@zzu.edu.cn.

Notes

The authors declare no competing financial interest.

■ ACKNOWLEDGMENTS

The work described in this paper was supported by the National Natural Science Foundation of China (No. 21303167) and China Postdoctoral Science Foundation (No. 2013M530340).

■ REFERENCES

(1) Arduengo, A. J., III; Harlow, R. L; Kline, M. *J. Am. Chem. Soc.* **1991**, *113*, 361−363.
(2) Herrmann, W. A. *Angew. Chem., Int. Ed.* **2002**, *41*, 1290−1309.
(3) Crudden, C. M.; Allen, D. P. *Coord. Chem. Rev.* **2004**, *248*, 2247−2273.
(4) Hahn, F. E.; Jahnke, M. C. *Angew. Chem., Int. Ed.* **2008**, *47*, 3122−3172.
(5) Díez-González, S.; Marion, N.; Nolan, S. P. *Chem. Rev.* **2009**, *109*, 3612−3676.
(6) Biju, A. T.; Kuhl, N.; Glorius, F. *Acc. Chem. Res.* **2011**, *44*, 1182−1195.
(7) Nair, V.; Menon, R. S.; Biju, A. T.; Sinu, C. R.; Paul, R. R.; Jose, A.; Sreekumar, V. *Chem. Soc. Rev.* **2011**, *40*, 5336−5346.
(8) Cohen, D. T.; Scheidt, K. A. *Chem. Sci.* **2012**, *3*, 53−57.
(9) DiRocco, D. A.; Noey, E. L.; Houk, K. N.; Rovis, T. *Angew. Chem.* **2012**, *124*, 2441−2444.
(10) Grossmann, A.; Enders, D. *Angew. Chem.* **2012**, *124*, 320−332.
(11) Dalko, P. I.; Moisan, L. *Angew. Chem., Int. Ed.* **2001**, *40*, 3726−3748.
(12) Dalko, P. I.; Moisan, L. *Angew. Chem., Int. Ed.* **2004**, *43*, 5138−5175.
(13) Seayad, J.; List, B. *Org. Biomol. Chem.* **2005**, *3*, 719−724.
(14) Enders, D.; Grondal, C.; Hüttl, M. R. M. *Angew. Chem., Int. Ed.* **2007**, *46*, 1570−1581.
(15) MacMillan, D. W. C. *Nature* **2008**, *455*, 304−308.

(16) Cheong, P. H. Y.; Legault, C. Y.; Um, J. M.; Celebi-Olcum, N.; Houk, K. N. *Chem. Rev.* **2011**, *111*, 5042−5137.
(17) Enders, D.; Niemeier, O.; Henseler, A. *Chem. Rev.* **2007**, *107*, 5606−5655.
(18) Marion, N.; Díez-González, S.; Nolan, S. P. *Angew. Chem., Int. Ed.* **2007**, *46*, 2988−3000.
(19) Enders, D.; Balensiefer, T. *Acc. Chem. Res.* **2004**, *37*, 534−541.
(20) Baragwanath, L.; Rose, C. A.; Zeitler, K.; Connon, S. J. *J. Org. Chem.* **2009**, *74*, 9214−9217.
(21) Ema, T.; Oue, Y.; Akihara, K.; Miyazaki, Y.; Sakai, T. *Org. Lett.* **2009**, *11*, 4866−4869.
(22) Enders, D.; Grossmann, A.; Fronert, J.; Raabe, G. *Chem. Commun.* **2010**, *46*, 6282−6284.
(23) Kankala, S.; Edulla, R.; Modem, S.; Vadde, R.; Vasam, C. S. *Tetrahedron Lett.* **2011**, *52*, 3828−3831.
(24) Jousseaume, T.; Wurz, N. E.; Glorius, F. *Angew. Chem.* **2011**, *123*, 1446−1450.
(25) Liu, F.; Bugaut, X.; Schedler, M.; Fröhlich, R.; Glorius, F. *Angew. Chem.* **2011**, *123*, 12834−12839.
(26) Piel, I.; Steinmetz, M.; Hirano, K.; Fröhlich, R.; Grimme, S.; Glorius, F. *Angew. Chem.* **2011**, *123*, 5087−5091.
(27) Li, Y.; Zhao, Z. A.; He, H.; You, S. L. *Adv. Synth. Catal.* **2008**, *350*, 1885−1890.
(28) Cohen, D. T.; Cardinal-David, B.; Roberts, J. M.; Sarjeant, A. A.; Scheidt, K. A. *Org. Lett.* **2011**, *13*, 1068−1071.
(29) Zhao, X.; DiRocco, D. A.; Rovis, T. *J. Am. Chem. Soc.* **2011**, *133*, 12466−12469.
(30) Lv, H.; Chen, X. Y.; Sun, L. H.; Ye, S. *J. Org. Chem.* **2010**, *75*, 6973−6976.
(31) Wang, X. N.; Zhang, Y. Y.; Ye, S. *Adv. Synth. Catal.* **2010**, *352*, 1892−1895.
(32) Ryan, S. J.; Candish, L.; Lupton, D. W. *J. Am. Chem. Soc.* **2011**, *133*, 4694−4697.
(33) Zhang, Y. R.; He, L.; Wu, X.; Shao, P. L.; Ye, S. *Org. Lett.* **2008**, *10*, 277−280.
(34) Huang, X. L.; Chen, X. Y.; Ye, S. *J. Org. Chem.* **2009**, *74*, 7585−7587.
(35) Wang, X. N.; Shen, L. T.; Ye, S. *Chem. Commun.* **2011**, *47*, 8388−8390.
(36) Sun, L. H.; Shen, L. T.; Ye, S. *Chem. Commun.* **2011**, *47*, 10136−10138.
(37) Fang, X.; Chen, X.; Chi, Y. R. *Org. Lett.* **2011**, *13*, 4708−4711.
(38) Jiang, K.; Tiwari, B.; Chi, Y. R. *Org. Lett.* **2012**, *14*, 2382−2385.
(39) Mo, J.; Chen, X.; Chi, Y. R. *J. Am. Chem. Soc.* **2012**, *134*, 8810−8813.
(40) Wei, D. H.; Zhu, Y. Y.; Zhang, C.; Sun, D. Z.; Zhang, W. J.; Tang, M. S. *J. Mol. Catal. A: Chem.* **2011**, *334*, 108−115.
(41) Zhang, W. J.; Zhu, Y. Y.; Wei, D. H.; Li, Y. X.; Tang, M. S. *J. Org. Chem.* **2012**, *77*, 10729−10737.
(42) Zhang, W. J.; Wei, D. H.; Tang, M. S. *J. Org. Chem.* **2013**, *78*, 11849−11859.
(43) Kuniyil, R.; Sunoj, R. B. *Org. Lett.* **2013**, *15*, 5040−5043.
(44) Fu, Z.; Sun, H.; Chen, S.; Tiwari, B.; Li, G.; Chi, Y. R. *Chem. Commun.* **2013**, *49*, 261−263.
(45) Xia, Y. Z.; Liang, Y.; Chen, Y. Y.; Wang, M.; Jiao, L.; Huang, F.; Liu, S.; Li, Y. H.; Yu, Z. X. *J. Am. Chem. Soc.* **2007**, *129*, 3470−3471.
(46) Shi, F. Q.; Li, X.; Xia, Y. Z.; Zhang, L. M.; Yu, Z. X. *J. Am. Chem. Soc.* **2007**, *129*, 15503−15512.
(47) Liang, Y.; Zhou, H. L.; Yu, Z. X. *J. Am. Chem. Soc.* **2009**, *131*, 17783−17785.
(48) Jiang, G. J.; Wang, Y.; Yu, Z. X. *J. Org. Chem.* **2013**, *78*, 6947−6955.
(49) Zhuo, L. G.; Zhang, J. J.; Yu, Z. X. *J. Org. Chem.* **2012**, *77*, 8527−8540.
(50) Peng, Q.; Yan, H.; Zhang, X. H.; Wu, Y. D. *J. Org. Chem.* **2012**, *77*, 7487−7496.
(51) Jiao, L.; Yu, Z. X. *J. Org. Chem.* **2013**, *78*, 6842−6848.
(52) Chen, K.; Xu, L. P.; Wiest, O. *J. Org. Chem.* **2013**, *78*, 5051−5055.
(53) Domingo, L. R.; Sáez, J. A.; Joule, J. A.; Rhyman, L.; Ramasami, P. *J. Org. Chem.* **2013**, *78*, 1621−1629.
(54) Breugst, M.; Grée, R.; Houk, K. N. *J. Org. Chem.* **2013**, *78*, 9892−9897.
(55) James, N. C.; Um, J. M.; Padias, A. B.; Hall, H. K.; Houk, K. N. *J. Org. Chem.* **2013**, *78*, 6582−6592.
(56) Lan, Y.; Danheiser, R. L.; Houk, K. N. *J. Org. Chem.* **2012**, *77*, 1533−1538.
(57) Wang, H.; Jain, P.; Antilla, J. C.; Houk, K. N. *J. Org. Chem.* **2013**, *78*, 1208−1215.
(58) Frisch, M. J.; Trucks, G. W.; Schlegel, H. B.; Scuseria, G. E.; Robb, M. A.; Cheeseman, J. R.; Scalmani, G.; Barone, V.; Mennucci, B.; Petersson, G. A.; Nakatsuji, H.; Caricato, M.; Li, X.; Hratchian, H. P.; Izmaylov, A. F.; Bloino, J.; Zheng, G.; Sonnenberg, J. L.; Hada, M.; Ehara, M.; Toyota, K.; Fukuda, R.; Hasegawa, J.; Ishida, M.; Nakajima, T.; Honda, Y.; Kitao, O.; Nakai, H.; Vreven, T.; Montgomery, J. A., Jr.; Peralta, J. E.; Ogliaro, F.; Bearpark, M.; Heyd, J. J.; Brothers, E.; Kudin, K. N.; Staroverov, V. N.; Kobayashi, R.; Normand, J.; Raghavachari, K.; Rendell, A.; Burant, J. C.; Iyengar, S. S.; Tomasi, J.; Cossi, M.; Rega, N.; Millam, J. M.; Klene, M.; Knox, J. E.; Cross, J. B.; Bakken, V.; Adamo, C.; Jaramillo, J.; Gomperts, R.; Stratmann, R. E.; Yazyev, O.; Austin, A. J.; Cammi, R.; Pomelli, C.; Ochterski, J. W.; Martin, R. L.; Morokuma, K.; Zakrzewski, V. G.; Voth, G. A.; Salvador, P.; Dannenberg, J. J.; Dapprich, S.; Daniels, A. D.; Farkas, Ö.; Foresman, J. B.; Ortiz, J. V.; Cioslowski, J.; Fox, D. J., Gaussian 09, Revision C.01; Gaussian, Inc.: Wallingford, CT, 2010.
(59) Zhang, W. J.; Zhu, Y. Y.; Wei, D. H.; Tang, M. S. *J. Comput. Chem.* **2012**, *33*, 715−722.
(60) Wei, D. H.; Lei, B. L.; Tang, M. S.; Zhan, C. G. *J. Am. Chem. Soc.* **2012**, *134*, 10436−10450.
(61) Wei, D. H.; Fang, L.; Tang, M. S.; Zhan, C. G. *J. Phys. Chem. B.* **2013**, *117*, 13418−13434.
(62) Wei, D. H.; Huang, X. Q.; Liu, J. J.; Tang, M. S.; Zhan, C. G. *Biochemistry* **2013**, *52*, 5145−5154.
(63) Becke, A. D. *J. Chem. Phys.* **1993**, *98*, 5648−5652.
(64) Lee, C.; Yang, W.; Parr, R. G. *Phys. Rev. B* **1988**, *37*, 785−789.
(65) Mennucci, B.; Tomasi, J. *J. Chem. Phys.* **1997**, *106*, 5151−5158.
(66) Barone, V.; Cossi, M. *J. Phys. Chem. A* **1998**, *102*, 1995−2001.
(67) Sun, L.; Tang, M. S.; Wang, H. M.; Wei, D. H.; Liu, L. *Tetrahedron: Asymmetry* **2008**, *19*, 779−787.
(68) Wei, D. H.; Tang, M. S.; Zhao, J.; Sun, L.; Zhang, W. J.; Zhao, C. F.; Zhang, S. R.; Wang, H. *Tetrahedron: Asymmetry* **2009**, *20*, 1020−1026.
(69) Legault, C. Y.; Garcia, Y.; Merlic, C. A.; Houk, K. N. *J. Am. Chem. Soc.* **2007**, *129*, 12664−12665.
(70) Parr, R. G.; Pearson, R. G. *J. Am. Chem. Soc.* **1983**, *105*, 7512−7516.
(71) Domingo, L. R.; Aurell, M. J.; Perez, P.; Contreras, R. *Tetrahedron* **2002**, *58*, 4417−4423.
(72) Domingo, L. R.; Saez, J. A.; Zaragoza, R. J.; Arno, M. *J. Org. Chem.* **2008**, *73*, 8791−8799.
(73) Domingo, L. R.; Picher, M. T.; Saez, J. A. *J. Org. Chem.* **2009**, *74*, 2726−2735.
(74) Domingo, L. R.; Saez, J. A. *Org. Biomol. Chem.* **2009**, *7*, 3576−3583.
(75) Kohn, W.; Sham, L. J. *Phys. Rev. B.* **1965**, *137*, 1697−1705.
(76) Kohn, W.; Sham, L. J. *Phys. Rev. B.* **1965**, *140*, 1133−1138.
(77) Sham, L. J.; Kohn, W. *Phys. Rev. B.* **1966**, *145*, 561−567.
(78) Domingo, L. R.; Chamorro, E.; Perez, P. *J. Org. Chem.* **2008**, *73*, 4615−4624.
(79) Domingo, L. R.; Chamorro, E.; Perez, P. *J. Phys. Chem. A.* **2008**, *112*, 4046−4053.
(80) Perez, P.; Domingo, L. R.; Duque-Norena, M.; Chamorro, E. *J. Mol. Struc.(Theochem)* **2009**, *895*, 86−91.
(81) Domingo, L. R.; Chamorro, E.; Perez, P. *Eur. J. Org. Chem.* **2009**, *2009*, 3036−3044.
(82) Domingo, L. R.; Perez, P.; Saez, J. A. *RSC Adv.* **2013**, *3*, 1486−1494.

(83) Domingo, L. R.; Perez, P.; Ortega, D. E. *J. Org. Chem.* **2013**, *78*, 2462−2471.
(84) Chamorro, E.; Perez, P.; Domingo, L. R. *Chem. Phys. Lett.* **2013**, *582*, 141−143.
(85) Zhao, Y.; Truhlar, D. G. *Theor. Chem. Acc.* **2008**, *120*, 215−241.
(86) Zhao, Y.; Truhlar, D. G. *Acc. Chem. Res.* **2008**, *41*, 157−167.